Methane production from ATJ graphite by slow atomic and molecular D ions: Evidence for projectile molecule-size-dependent yields at low energies

L.I. Vergara [a,*], F.W. Meyer [a,*], H.F. Krause [a], P. Träskelin [b],
K. Nordlund [b], E. Salonen [c]

[a] *Physics Division, Oak Ridge National Laboratory, Oak Ridge, TN 37831-6372, USA*
[b] *University of Helsinki, Accelerator Lab, P.O. Box 43, Helsinki, FIN-00014, Finland*
[c] *Helsinki University of Technology and Helsinki Institute of Physics, P.O. Box 1100, FIN-02015 HUT, Finland*

Abstract

We present experimental results for methane production from ATJ graphite impacted by atomic and molecular D ions in the energy range 5–60 eV/D. A systematic trend of the methane yields for the different molecular species compared at the same impact energy/D is observed: while all three species lead to methane yields that coincide within the experimental uncertainty at the high energy end of the investigated range, at lower energies the yields diverge by progressively larger amounts, with the incident triatomic molecular ion leading to the largest yields per atom, and the atomic ion to the smallest. The difference at the lowest investigated energy (10 eV/D) is about a factor of two. Total chemical sputtering yields obtained by classical molecular dynamic simulations also indicate that molecular projectiles lead to larger yields per atom than atomic projectiles. The energy dependence of the total yield increase obtained by the simulations, however, is different than that observed experimentally for methane production.
© 2006 Published by Elsevier B.V.

PACS: 34.50.Dy; 52.20.Hv; 79.20.−m; 79.20.Rf

1. Introduction

Because of its high thermal conductivity, excellent shock resistance, absence of melting, low activation, and low atomic number, there is significant technological interest in using graphite as a plasma-facing component on present and future fusion devices. This interest extends to the use of different types of graphite or carbon fiber composites (CFCs) in the ITER divertor. Although these materials have outstanding thermo-mechanical properties, they can suffer significant chemical erosion and sputtering by low energy hydrogen ion impact, which determines in large part the

---

* Corresponding authors. Tel.: +1 865 574 4781; fax: +1 865 574 1118 (L.I. Vergara), tel.: +1 865 574 4705; fax: +1 865 574 1118 (F.W. Meyer).

E-mail addresses: vergarali@ornl.gov (L.I. Vergara), meyerfw @ornl.gov (F.W. Meyer).

carbon-based-material lifetime. Due to evolving divertor design, the interest in the erosion characteristics of the carbon surfaces is shifting to progressively lower impact energies. To reach the required low energies, laboratory measurements of relevant chemical sputtering yields have, for technical reasons, relied increasingly on the use of molecular hydrogen beams to simulate atomic hydrogen impact. This is based on the experimental finding that, at high energies and elevated sample temperatures, atomic and molecular projectiles with the same energy/D resulted in identical sputtering yields, after normalization to the number of hydrogen atoms in the incident projectile [1]. The question whether this equivalence holds at lower energies and room temperature samples as well, however, has, to our knowledge, not yet been experimentally or theoretically addressed.

Motivated in part by this issue, an experimental research program was recently started at the ORNL Multicharged Ion Research Facility (MIRF) [2] to investigate chemical sputtering of graphite surfaces in the limit of very low impact energies, where there is currently little experimental data [3]. To date, many studies of chemical sputtering of graphite with low-energy beams have been reported (Refs. [4–11], among others). However, without exception, these studies used molecular instead of atomic beams at the lower impact energies ($\leqslant 30$ eV/D), since fluxes

of atomic projectile beams were too low to permit reliable measurements of the progressively smaller sputtering yields with decreasing energy. The sputtering yield results were then quoted per incident H or D atom at energies obtained by dividing the impacting molecular projectile kinetic energy by the number of constituent H or D atoms, i.e. by making the assumption that atomic and molecular projectiles at the same energy/D lead to the same sputtering yield per atom in the investigated energy range. In the present paper, we investigate the validity of this assumption for CD_4 production resulting from atomic D^+ and molecular D_x^+ ion impact on room temperature graphite in the energy range 5–60 eV/D.

2. Experiment

All measurements were performed in a floating potential ultra-high vacuum chamber with base pressures in the 10^{-8} Pa range, into which decelerated ion beams from an ECR ion source were directed, as described elsewhere [12]. A sensitive quadrupole mass spectrometer was installed in the scattering chamber as shown in Fig. 1. A grounded baffle between the front end of the QMS and the target sample prevented field penetration from the QMS ionizer section into the region immediately in front of the sample where the low energy ion
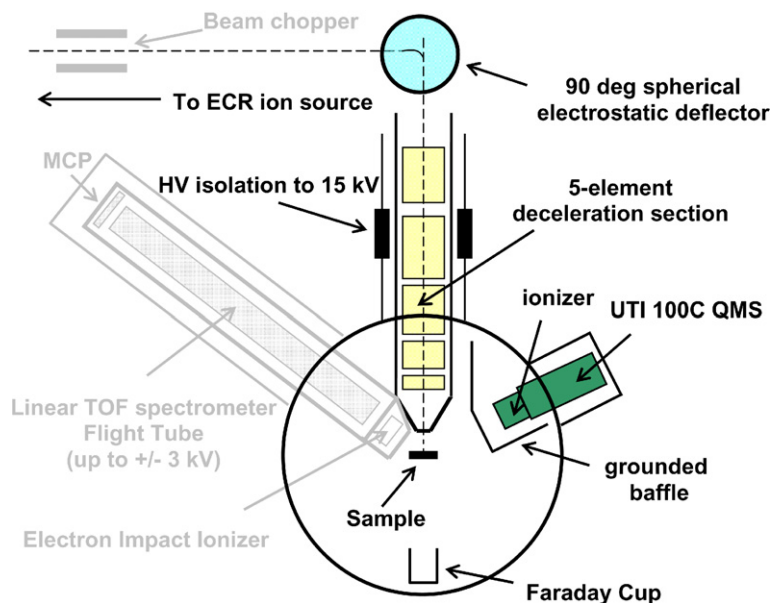

Fig. 1. Schematic diagram of the decelerated beam surface scatttering apparatus. The highlighted parts are the relevant ones for the present experiments.
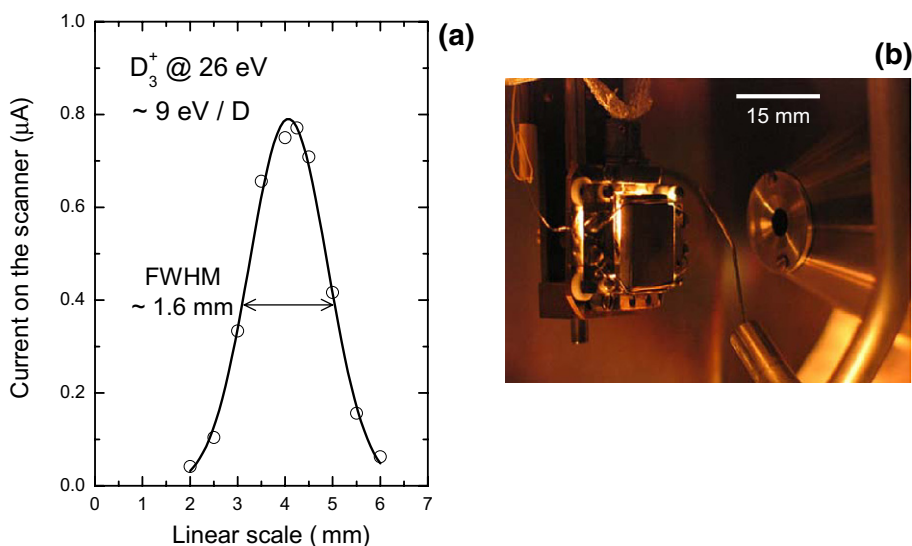
Fig. 2. (a) Typical spatial profile of the decelerated beams. (b) Photograph of the interior of the scattering chamber, showing the wire beam scanner, and the sample holder located in the retracted position used during the beam profile measurements. During target irradiation, the wire is retracted, and the sample is rotated 90° toward the beam after translation to the scanner position. The sample is a 15×12 mm tile.

beam hit the graphite target. This baffle also blocked the line-of-sight path between the sample and the analyzer, along which scattered projectiles at higher beam energies could enter and cause unwanted background contributions to the measured mass spectra. The chamber also housed a time-of-flight analyzer previously used for binary-collision backscattering studies [13], which was not used in the present experiment.

A target fabricated from ATJ graphite (UCAR Carbon Co.), a low-density form of graphite ($\sim$1.7 g/cm^3), was used for all measurements. This is the same material presently employed on the DIII-D device at General Atomics [10]. Prior to mounting, the target was pre-annealed for at least 4 h at a temperature of 1300 K in a vacuum furnace. For the experiment, the target temperature variation was achieved by electron-beam-heating from the rear, and was monitored from the front using a calibrated infrared (IR) thermal monitor. Annealing at temperatures in excess of 1500 K was performed for about 45 s between measurements in order to reinitialize the H/D inventory in the graphite sample. The sample was located 15 mm downstream from the final aperture of the electrostatic deceleration system. For all measurements, the mass-selected projectile beam impacted the sample at normal incidence. When working with D$^+$ and D$_2^+$ beams, the incident ion beam spatial profile is

approximately Gaussian with a width in the range 1–2 mm (FWHM) for energies down to 30 eV/D, and about 5 mm for the 15 and 10 eV/D beams. In the case of D$_3^+$ beams, widths <2 mm were also obtained for energies lower than 10 eV/D, as illustrated in Fig. 2(a). The profiles were determined by a wire scanner that could be inserted in the plane of the target sample as shown in Fig. 2(b). Using the beam currents intercepted by the sample and the beam profile measurements, typical beam fluxes of 2–8×10^{19} D/(m^2 s) were determined down to 30 eV/D. Fluxes in excess of 1×10^{18} D/(m^2 s) were obtained down to the lowest investigated energies. The incident ion intensity was determined from the direct current reading on the sample, after making the appropriate correction for secondary electron emission. This correction was based on in situ measurements for a few selected incident species and energies, and on the scaling with projectile energy and mass reported in Ref. [14]. The energy spread of the decelerated beams was determined to be $\sim$3 eV. This estimate was obtained by measuring the sample current as function of a small bias voltage applied to the scattering chamber with respect to the ECR ion source voltage, until zero current was reached. A polynomial fit to the entire retardation curve (solid curve with data points in Fig. 3) includes the energy spread due to finite ion temperature in the ECR source. A second fit excluding the
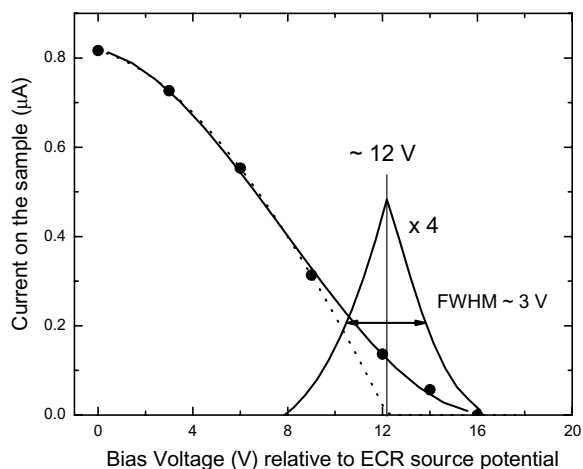
Fig. 3. Measurement of the current on the sample vs. bias voltage (relative to the ECR ion source voltage) applied to decelerate the incident beam. Solid line through data points: polynomial fit of the experimental data points. Dotted line: polynomial fit excluding points affected by ion source temperature effects. The intersection of this curve with the *x*-axis provides an estimate of the plasma potential (∼12 V in this case). Subtraction of the two fits gives an estimation of the incident beam energy-spread: solid line without data points.

region dominated by source ion temperature effects provides an estimate of the source plasma potential (see dashed curve in Fig. 3), which in this case was found to be approximately 12 V. The difference between the two curves gives the energy spread (solid curve without data points). While this approach gave energy spread values somewhat larger than those obtained from earlier measurements of decelerated beam properties using a hemispherical analyzer (see e.g. Ref. [2]), such an increase is to be expected, since the earlier measurements sampled only a small fraction of the incident beam, while the present measurements were made with the entire impacting beam. Typical vacuum during the measurements (i.e. with decelerated beam in the UHV chamber) was in the mid 10^{-7} Pa range.

The present experimental approach for the detection of the hydrocarbon reaction products uses a sensitive quadrupole mass spectrometer which monitors the partial pressure of selected mass species in the scattering chamber throughout the 1–60 amu range. A Macintosh-based data acquisition system is used to measure mass distributions at fixed intervals in time, or alternatively, to follow the intensity of selected mass peaks vs. beam exposure time. The evolution of peak intensities is measured vs. accumulated beam dose until saturation occurs. It is crucial to the experimental approach that all contri-

butions to the chamber pressure other than those related to the incident beam be kept constant during the irradiation runs. This allows the evolution of chemical sputtering products to be determined by taking differences between a pre-irradiation mass spectrum and one acquired during irradiation at progressively larger accumulated D target doses.

3. Estimation of hydrocarbon yields

The procedure used to deduce the partial chemical sputtering yields, i.e. the different hydrocarbon production yields, was adapted from [5] and is described in Refs. [15,16]. It involves selection of an analysis mass for each species of interest (in the present case CD_4), determining and correcting for the possible interferences due to cracking of heavier hydrocarbons, and placing the production yields on an absolute scale using calibrated leaks. The procedure is expressed by the following equation [16]:

$$\underline{y} = \mathbf{R}(\mathbf{C}^{-1}\underline{s}), \tag{1}$$

where $\underline{y}$ is the apparent production yield array for the selected hydrocarbons, $\mathbf{C}$ is the cracking pattern matrix, and $\mathbf{R}$ is the diagonal calibration matrix giving the conversion from QMS normalized peak height to production rate in particles/s. The vector $\underline{s}$ is the array of measured peak heights (normalized to the incident ion flux, expressed in particles/s) at each analysis mass.

To obtain true partial chemical sputtering yields, the apparent yields must be corrected for wall contributions. This wall effect can arise when the fraction of the incident deuterium beam reflected from the graphite target combines with hydrocarbon precursors on the interior vacuum chamber walls to form the products of interest. As discussed in Ref. [7], such wall contributions can be estimated from the initial steep rise observed in the signal immediately after initiation of beam irradiation, since the deuterium concentration in the graphite at that point is still too low to directly produce appreciable chemical sputtering products. Typical examples of wall contribution signatures in the time dependent CD_4 signal obtained in the present experiment can be found in Refs. [15,16].

4. Molecular dynamics simulation method

To understand the mechanisms behind the experimental results, classical molecular dynamic (MD)

simulations were performed. The simulations were carried out on three different GRID Linux clusters of the University of Helsinki and Center for Scientific Computing, using the HCPARCAS simulation code in a manner previously described [17,18]. Briefly, the interatomic forces were calculated using the empirical Brenner–Beardmore many-body potential [19]. A simulation cell consisting initially of 1000 atoms was prepared with a D/C ratio of 0.4, matching the experimental deuterium saturation value of bulk a-C:D at 300 K [20,21]. The fractions of sp^2 and sp^3 hybridized carbon atoms in the cell, including surface atoms, were 50–65% and 25–40%, respectively, and the density of the cell about 2.1 g/cm^3. The atoms within a distance of 2 Å from the bottom of the cell were held fixed and the atom layers at the sides and closest to the fixed bottom layers were scaled towards a temperature of 300 K to remove the excess heat introduced by the impinging ions. Periodic boundary conditions were applied in the directions perpendicular to the surface normal. D, D_2 or D_3 projectiles were placed outside the simulation cell, rotated randomly, and shot perpendicularly towards it with kinetic energies in the range 2–30 eV/atom. In the interaction model used, the D_2 molecule has the experimental bond length, a binding energy of 4.751 eV and the (classical) ground state vibration frequency [19]. The D_3 molecule can be stabilized in the Brenner model in an isosceles triangle shape with one strong, short and two weak, long 'bonds', with a binding energy of 4.753 eV. We use this structure as the closest possible approximation to the experimentally used D_3 radical (charge states are not included in a classical MD simulation). Each bombardment event was followed for 2 ps (some simulations were also run with a time of 4 ps, and found to give the same results within the uncertainties as the 2 ps results). The carbon sputtering yield was determined by carrying out an atom connectivity cluster analysis of all atoms above the simulation cell, using the bond lengths of the potential to determine which atoms were part of the same cluster. Clusters (i.e. atoms or molecules) which were not bound to the bulk simulation cell were labeled sputtered. At least 1000 events were simulated for each energy and projectile, for six different simulated surfaces. These surfaces were constructed by taking the initially prepared simulation cell, and rotating it six ways to expose each of its six surfaces in turn to the incident beam. The surface used for each impact was always the originally prepared surface and thus did not reflect the modi-

fication produced by prior impacts. Previous simulation work has found that there is some dependence of the quantitative results [22,23] on the interatomic interaction model used. However, all qualitative trends in sputtering have been found to be independent of the chosen model.

The present simulations and experimental measurements differ in three main aspects: (i) in the present experiments only the CD_4 production yield was measured, while in the simulations the total C sputtering yield is obtained; (ii) the measurements start from a polycrystalline ATJ graphite surface (which most likely becomes more amorphous during the irradiation), while the simulations are carried out on an initially completely amorphous sample (the latter sample is more likely to have loosely bound surface hydrocarbon groups which sputter easily; simulating sputtering for the low-density graphite structure used in the present measurements was not possible due to prohibitively long simulation times of the H buildup that would have been required), and (iii) in the measurements, the near surface hydrogenation depth varies with incident projectile energy (since it is the impacting beam which performs the hydrogenation), while the simulations use the same prepared cell over the whole energy range. Thus, for the measurements there is most likely a greater concentration of methyl precursors at the surface or near surface region at the lowest measured energies than at the high end of the investigated energy range. Regarding the simulations, it is also noted that, for technical reasons and to confine the projectile penetration to the near surface region, i.e. away from the bottom cell boundary, the maximum energy that could be simulated is about 30 eV/D.

5. Results and discussion

5.1. Experimental results

Fig. 4 summarizes our methane production yields using atomic and molecular beams that impact on ATJ graphite at room temperature. The yields were normalized to the number of incident D atoms in each case. As can be seen from the figure, a systematic trend of the partial sputtering yields for the different molecular species compared at the same energy/D is evident. While all three species lead to partial chemical sputtering yields that agree within the experimental uncertainty at 60 eV/D, as has also been observed by Balden and Roth [8] for D^+ and
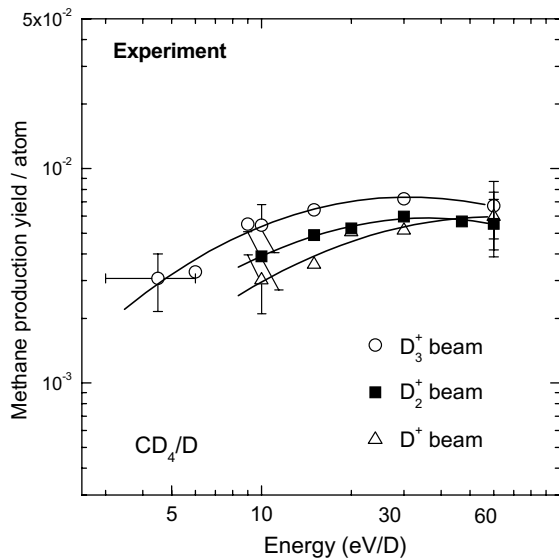
Fig. 4. Measured methane production yields per atom for three different beams impinging on ATJ graphite at room temperature: (○) D_3^+ beam, (■) D_2^+ and (△) D^+ beam, as function of the energy per D of the incident projectiles. The solid lines were drawn to guide the eye. For a better view, at 10 eV/D the error bars were shifted sideways.

D_3^+ beams at 50 eV/D, at lower energies the yields diverge by progressively larger amounts with decreasing energy. The incident triatomic molecular ions lead to the largest yields, and the atomic ions to the smallest. The difference at 10 eV/D (the lowest energy where yields were measured for all three incident ions) is about a factor of two.

Projectile mass dependences of chemical erosion yields for room temperature pyrolytic graphite have previously been found by Mech et al. [6,7] and Roth et al. [4,8]. Using a mass spectrometry approach, Mech et al. found an isotopic effect on both partial chemical erosion yields (e.g. methane production) and total chemical erosion yields (i.e. summed over all products). Both in the case of methane production and total erosion yields in the energy range 10–200 eV, they found yields that were systematically smaller for H incident beams than the corresponding ones for incident D, by factors ranging from a little over 1–2, depending on energy. A complication in interpreting those measurements in the present context is that the H measurements were performed with H_3^+ beams, while the D measurements were made with D_2^+ beams. Using a weight loss measurement approach, Roth and Bohdansky [4] and later Balden and Roth [8], working with H_3^+ and D_3^+ beams, showed an isotope effect on

the total erosion yields of graphite of about a factor of 5, significantly larger than the effect observed by Mech et al. [7].

Since the chemistry leading to the hydrocarbon production is independent of the incident isotope, it has been proposed that the observed yield differences arise from the mass differences of the isotopes [7,8]. The maximum energy transfer between a projectile of mass m_1 and energy E_{inc} and a target atom of mass m_2 in an elastic binary collision is given by the relation

$$E_{max} = \frac{4m_1 m_2}{(m_1 + m_2)^2} E_{inc}. \tag{2}$$

As a result, a higher mass projectile can produce more damage to the surface, thereby providing more open bonds for deuterium attachment. This in turn increases the probability of hydrocarbon production. In addition, higher mass projectiles can transfer more energy to methyl groups weakly attached to the surface, and thus are more likely to contribute to their kinetic ejection. Both the damage creation and ejection mechanisms are of particular importance for samples at room temperature, i.e. below the temperature thresholds of additional thermally activated processes that, at higher temperatures, can contribute significantly to and even dominate these two important steps in the chemical sputtering cycle [24,25]. This energy transfer mechanism responsible for the observed isotope effect has subsequently been confirmed by MD simulation studies [18] that compared chemical sputtering yields for H, D, and T atomic projectiles in the energy range 2–35 eV, and consistently found progressively higher yields as the mass of the hydrogen isotope was increased. The magnitude of the isotope effect found in going from H to T projectiles fluctuated between a factor of 1.4 and 4, and that found in going from H and D projectiles between 1.3 and 3, reflecting, in part, significant statistical uncertainty in the results at each investigated energy.

Returning to the present experimental results, if dissociation is not immediate upon impact on the surface, i.e. it does not occur in the first binary collision, then it is possible that the mass dependence of the maximum energy transfer underlying the just described isotope effects in the chemical sputtering yields, may help to explain, at least in part, the yield differences observed at low impact energies for the different incident atomic and molecular ions as well.

5.2. Molecular dynamics calculation

The molecular dynamics simulation results for total chemical sputtering yields obtained with D, D_2, and D_3 incident projectiles, averaged over the six different surfaces mentioned in Section 4, are presented in Fig. 5, and clearly show that the molecular projectiles lead to higher yields per atom than the incident atomic projectiles, and that the increase becomes larger as the number of atomic constituents in the molecule increases. This trend is reflected in the individual results for each of the six surfaces as well, demonstrating that the yield increase occurs irrespective of detailed surface structure (the yield variations between different individual surfaces were large, reflecting the differences in the number of loosely bound hydrocarbon species each surface had). The fact that the same trend, i.e. larger yields per atom for molecular vs. atomic projectiles, is observed in both the classical MD simulation results and in our experimental results for CD_4 production, strongly suggests that at least part of the differences in the yields for the different beams (D^+, D_2^+, and D_3^+) can be explained by classical energy-transfer processes.

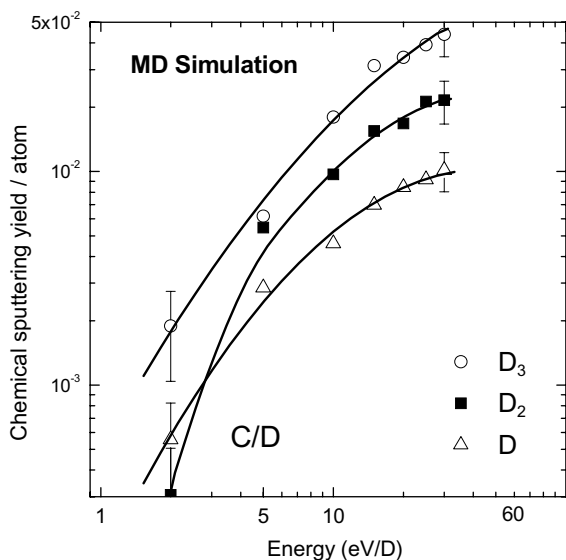It should be noted that while both experiment and MD simulations indicate higher yields per atom for incident molecular ions than for incident atomic ions, the measurements were made for methane production, while the simulation results represent a summation over all hydrocarbon products. It is not possible to ascertain at present to what extent this explains the different energy dependences of the yield increases in going from atomic to molecular projectiles evident in the measurements and simulations. In the experiments, the methane production yields per atom for D^+, D_2^+, and D_3^+ incident projectiles are roughly equal at 60 eV/D, while up to a factor of two higher yields were seen for incident D_3^+ than for D^+ at the lowest measured energy of 10 eV/D. For the MD simulations, the total yield increase in going from D to D_2 to D_3 projectiles ranges between a factor of two to five over the entire investigated energy range.

The observed trend, i.e. larger yields per atom for molecular vs. atomic projectiles, suggests that, at sufficiently low incident energies, molecular D_2^+ or D_3^+ ions incident on the graphite surface survive a significant part of the multiple collision cascade without dissociation. Our classical MD simulations confirm that this is indeed the case for the neutral molecules. We monitored the time evolution of trajectories of both D atoms of an incoming D_2 projectile and sputtered C atoms in individual MD simulations. The trajectories showed that in a large fraction of the events leading to sputtering, the D atoms were still bound or close to each other when the C atom started moving. This is illustrated in Fig. 6 for one particular case, which corresponds to a 20 eV D_2 impact event leading to sputtering. At 0.123 ps (Fig. 6(a)) the two D atoms are still bound, and jointly putting the C atoms in motion (Fig. 6(b)). The excitation of the lattice causes carbon–carbon bond breaking, which results in C atoms sputtering from the sample (Fig. 6(c) and (d)). The trajectories of one of the D atoms and both C atoms are not straight after sputtering because they are bound in molecules to other atoms which are not shown in Fig. 6. In the impact events leading to sputtering, complete dissociation does not occur until depths of 0.2–0.3 nm, and occasionally depths as great as 0.5 nm, have been reached.

It is noted that the yield increases with increasing incident molecule constituency number found in the present simulations exceed somewhat those found in our earlier isotope effect simulations [18]. In the energy range 5–60 eV/D, the yield increase in going from D to D_3 ranges from a factor of two to five. The difference in the simulations could be due to

Fig. 5. MD simulation results for the chemical sputtering yields per atom of graphite (a-C:D) by incident D, D_2 and D_3 projectiles. The data are averages over six different surfaces (see text). The uncertainty is the standard error of the mean of the results obtained for the different surfaces. The solid lines were drawn to guide the eye.
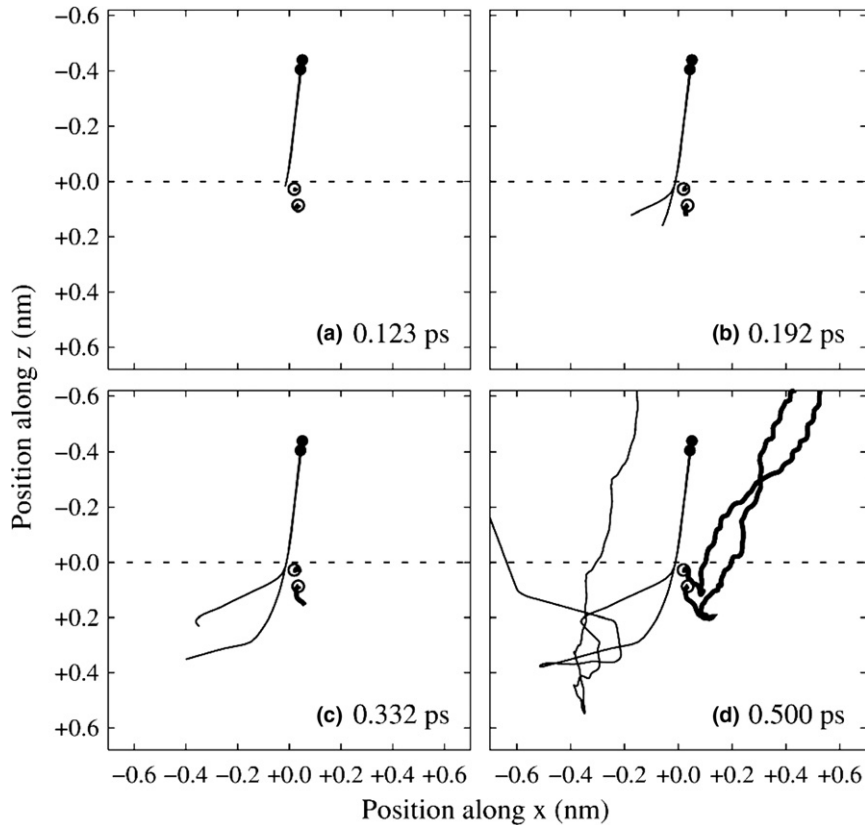
Fig. 6. Trajectories of atoms in a 20 eV D_2 impact event leading to sputtering. For clarity, only the two incoming D atoms of the incident D_2 projectile and the two sputtered C atoms are shown. The initial positions of the two D atoms and the C atoms are shown with solid and open circles, respectively. The D and C trajectories are shown with thin and thick lines, respectively. Each frame shows the trajectories up to the time indicated in the lower right corner.

the change in the maximum energy transfer (Eq. (2)), when taking into account that, in case of the different isotopes, the mass of the sputtered particles increases (e.g. mass 16 for CH_4 to mass 24 for CT_4) together with projectile mass, while for the different incident molecules, the sputtered particle mass stays fixed. Thus for the different isotopes, the maximum energy transfer increases from 22% to 39% going from H/CH_4 to T/CT_4, while this quantity increases from 33% to 71% going from D/CD_4 to D_3/CD_4. Similar effects are obtained for other precursors on the surface (CH_x or CD_x in general). This increase in energy transfer alone most likely does not fully explain the yield increase, since, for the molecular projectiles, the yields are already divided by the number of D constituents per incident molecule. Additional factors indeed may contribute to the observed enhancement. For example, it is possible that two or three atoms in close proximity, i.e. bound, can disturb the graphite lattice and cause

bond-breaking to a greater extent than a single atom of equivalent mass, thus leading to higher sputtering yields. Also, the individual D atoms may cause additional sputtering after breakup. Furthermore, while the results are plotted in units of eV/D, the total impact kinetic energy for D_2^+ and D_3^+ incident projectiles is, in fact, two or three times that of the corresponding incident D^+ case, respectively. Finally, our simple energy transfer argument ignores the possibility that there is a threshold energy transfer in the vicinity of which the chemical sputtering yields will not depend linearly on E_{max}, e.g. where the increase from 33% to 71% may be the crucial increase needed to exceed the threshold.

5.3. Comparison of experimental results and MD calculations

An obvious difference between the experimental and simulation results is the gradual disappearance

of the molecular size enhancement in the measured yields with increasing projectile energies, which is not apparent in the simulation results. This difference may be related to the earlier noted energy dependent hydrogenation layer thickness in the case of the measurements, which may have as a consequence that the concentration of erosion precursors at the surface increases with decreasing energy. In this case, the probability of an incident molecule having an encounter with such a precursor as its first binary collision with the surface, i.e. prior to dissociation, thereby kinetically desorbing it, is largest at the lowest energies, and gradually decreases with increasing energy, leading to gradual disappearance of the enhancement. Such an energy dependent 'activated' layer thickness is not considered in the simulations.

The classical MD simulations do not include electronic processes such as Auger or resonant neutralization, and dissociative electron capture [26], both of which are expected to be important in the energy range of the present investigation. However, even with the inclusion of dissociative electron capture, dissociation of the incident molecular ion would not be immediate, since, e.g. in the case of D_2^+, there is a finite chance of the electron capture occurring into a non-dissociating state. As a result, the molecular size effects discussed above would still take place until the dissociation occurs. For a more comprehensive understanding, it would be interesting to incorporate such electronic processes into MD simulations to see what their overall effect on the chemical sputtering yields is. Such an extension of the MD approach is currently under investigation [27].

6. Conclusions

In order to test the validity of the often used assumption that atomic and molecular projectiles at the same energy/D lead to identical chemical sputtering yields at low impact energies and room temperature samples, we have performed measurements of the methane (CD_4) production yield resulting from the impact of D, D_2^+, and D_3^+ ion beams normally incident on ATJ graphite at room temperature for beam energies in the range 5–60 eV/D, and MD simulations of total chemical sputtering yields for the same three projectiles and energies up to 30 eV/D.

Based on both our measurements and the simulations, we conclude that this assumption breaks down at energies below 60 eV/D when using molecular D projectiles. While equal within the experimental uncertainty at 60 eV/D, the measured CD_4 yields per atom for D^+, D_2^+, and D_3^+ projectiles at lower energies differ by increasing amounts as the impact energy per D is decreased, with the incident triatomic molecular ion leading to the largest yields per atom, and the atomic ion to the smallest. The difference at the lowest investigated energy is about a factor of two. Classical molecular dynamics simulations of the total chemical sputtering yields also indicate that molecular projectiles lead to larger yields per incident atom than atomic projectiles. However, the energy dependences of the experimentally determined methane production yields for atomic and molecular projectiles are different from the calculated MD total chemical sputtering yields. The experimental methane production yields overlap within experimental error for all three incident projectiles at 60 eV/D, and differ by as much as a factor of two at the lowest measured energy of 10 eV/D; for the MD simulations, the total yield increase in going from D to D_3 incident projectiles is consistently higher, by factors of two to five, over the entire energy range studied.

An extended study of the time evolution of trajectories of both D atoms of an incoming D_2 projectile and sputtered C atoms in individual MD simulations showed that in a significant fraction of the events leading to sputtering, the D atoms could still be bound or close to each other. These results strongly suggest that a major part of the differences in the yields for the different beams (D^+, D_2^+, and D_3^+) can be explained by classical energy-transfer processes, which contribute to the kinetic desorption of the erosion precursors.

This effect may, at least in part, explain the differences in isotope effects observed by Mech et al. [6,7] and Roth and co-workers [4,8]. Using H_3^+ and D_2^+ beams (Mech et al.), the increase in maximum energy transfer (from Eq. (2)) is only about 2.4%, while in the case of H_3^+ and D_3^+ (Roth et al.) the maximum energy transfer increase is more than an order of magnitude greater (33.5%). The possibility of intact molecular projectiles enhancing kinetically assisted desorption of erosion products from the graphite surface, therefore can interfere with the isolation and quantitative assessment of other projectile-mass-related effects such as the H/D/T isotope effect. For unambiguous identification and quantification of the latter effect, the use of atomic projectiles is thus highly recommended.

References

[1] R. Yamada, J. Nucl. Mater. 145–147 (1987) 359.
[2] F.W. Meyer, in: J. Gillaspy (Ed.), Trapping of Highly Charged Ions: Fundamentals and Applications, Nova Science, New York, 2000, p. 117. Available from: <http://www.phy.ornl.gov/atomic/MIRF/Facility.htm>.
[3] F.W. Meyer, L.I. Vergara, H.F. Krause, Phys. Scr. T124 (2006) 44.
[4] J. Roth, J. Bohdansky, Nucl. Instrum. and Meth. B 23 (1987) 549.
[5] J.W. Davis, A.A. Haasz, P.C. Stangeby, J. Nucl. Mater. 155–157 (1988) 234.
[6] B.V. Mech, A.A. Haasz, J.W. Davis, J. Nucl. Mater. 241–243 (1997) 1147.
[7] B.V. Mech, A.A. Haasz, J.W. Davis, J. Nucl. Mater. 255 (1998) 153.
[8] M. Balden, J. Roth, J. Nucl. Mater. 280 (2000) 39.
[9] E. Vietzke, J. Nucl. Mater. 290–293 (2001) 158.
[10] G.M. Wright, A.A. Haasz, J.W. Davis, R.G. Macaulay-Newcombe, J. Nucl. Mater. 337 (2005) 74.
[11] A.A. Haasz, B.V. Mech, J.W. Davis, J. Nucl. Mater. 231 (1996) 170.
[12] V.A. Morozov, F.W. Meyer, Rev. Sci. Inst. 70 (1999) 4515.
[13] V.A. Morozov, F.W. Meyer, Phys. Rev. Lett. 86 (2001) 736.
[14] S. Cornusca, A. Diem, H.P. Winter, F. Aumayr, J. Lörincik, Z. Sroubek, Nucl. Instrum. and Meth. B 193 (2002) 616.
[15] F.W. Meyer, H.F. Krause, L.I. Vergara, J. Nucl. Mater. 337 (2005) 922.
[16] L.I. Vergara, F.W. Meyer, H.F. Krause, J. Nucl. Mater. 347 (2005) 118.
[17] E. Salonen, Molecular dynamics studies of the chemical sputtering of carbon-based materials by hydrogen bombardment, PhD Thesis, University of Helsinki Report Series in Physics, HU-P-D97, 2002. Available from: <http://ethesis.helsinki.fi/>.
[18] E. Salonen, K. Nordlund, J. Keinonen, C.H. Wu, Phys. Rev. B 63 (2001) 195415;
E. Salonen, K. Nordlund, J. Keinonen, C.H. Wu, J. Nucl. Mater. 290–293 (2001) 144.
[19] D.W. Brenner, Phys. Rev. B 42 (1990) 9458;
Phys. Rev. B 46 (1992) 1948;
K. Beardmore, R. Smith, Phil. Mag. A 74 (1996) 1439.
[20] J. Roth, B.M.U. Scherzer, R.S. Blewer, D.K. Brice, S.T. Picraux, W.R. Wampler, J. Nucl. Mater. 93&94 (1980) 601.
[21] B.L. Doyle, W.R. Wampler, D.K. Brice, J. Nucl. Mater. 103&104 (1981) 513.
[22] E. Salonen, Phys. Scr. T 111 (2004) 113.
[23] A.V. Krasheninnikov, K. Nordlund, E. Salonen, J. Keinonen, C.H. Wu, Comput. Mater. Sci. 25 (2002) 427.
[24] J. Roth, C. Garcia-Rosales, Nucl. Fusion 36 (1996) 1647.
[25] B.V. Mech, A.A. Haasz, J.W. Davis, J. Appl. Phys. 84 (1998) 16.
[26] R. Janev, P. Krstic, Phys. Scr. T124 (2006) 96.
[27] P. Krstic, C.O. Reinhold, S.J. Stuart, private communication.